The eXact integral simplified time-dependent density functional theory (XsTD-DFT)

Marc de Wergifosse[†‡*], Stefan Grimme[‡]

[†]Theoretical Chemistry Group, Molecular Chemistry, Materials and Catalysis Division (MOST), Institute of Condensed Matter and Nanosciences, Université Catholique de Louvain, Place Louis Pasteur 1, B-1348 Louvain-la-Neuve, Belgium

[‡]Mulliken Center for Theoretical Chemistry, Institut für Physikalische und Theoretische Chemie, Beringstr. 4, 53115 Bonn, Germany

[*]marc.dewergifosse@uclouvain.be

ABSTRACT

In the framework of simplified quantum chemistry methods, we introduce the eXact integral simplified time-dependent density functional theory (XsTD-DFT). This method is based on the simplified time-dependent density functional theory (sTD-DFT) where all semi-empirical two-electron integrals are replaced by exact one- and two-center atomic orbital (AO) two-electron integrals while all other approximations from sTD-DFT are kept. The performance of this new parameter-free XsTD-DFT method was benchmarked to evaluate excited state and (non)linear response properties, including ultra-violet/visible absorption, first hyperpolarizability, and two-photon absorption. For a set of 77 molecules, results from the XsTDA approach (or XsTD-DFT considering the Tamm-Dancoff approximation) were compared to corresponding TDA data. XsTDA/B3LYP excitation energies only deviate absolutely by 0.14 eV in average from those obtained from standard TDA while drastically cutting computational costs by a factor of 20 or more depending on the single energy threshold chosen. The absolute deviations of excitation energies with respect to the full scheme are decreasing when the system size is increasing, showing the suitability of XsTDA/XsTD-DFT to treat large systems. Comparing XsTDA and its predecessor sTDA, the new scheme globally improves excitation energies and oscillator strengths. Particularly, the XsTDA scheme can faithfully reproduce TDA results for charge transfer states. Among the various results, TD-DFT first hyperpolarizability frequency dispersions for a set of push-pull π-conjugated molecules are faithfully reproduced by XsTD-DFT while the sTD-DFT method always provides red-shifted resonance energy positions. Excellent performance with respect to experiment is observed for the 2PA spectrum of the enhanced green fluorescent protein (eGFP). The generally excellent results with an accuracy similar to TD-DFT but at a fraction of its computational cost opens the way for a plethora of applications considering large systems as well as high throughput screening studies.

I. INTRODUCTION

The computation of molecular properties involving the interaction of light with matter using quantum chemistry (QC) methods remains challenging for large systems that are of timely interest. An ideal method should enable the treatment of open shell systems that may present multi-configurational character[1,2] and be able to compute excitations in vertical and adiabatic regimes. Considering linear and nonlinear optical response properties, the computation of such higher-order quantities is computationally-involved and often needs a proper treatment of electron correlation effects, frequency dispersion, and explicit account for the environment.[3,4] Such methods exist but only for small systems. If used with care, the time-dependent density functional theory (TD-DFT)[5–8] provides a reasonable route for the computation of excited states and response properties for medium-sized systems. However, it introduces substantial errors for several types of excitations involving charge-transfer (CT), double excitation, or Rydberg characters when using standard exchange-correlation (XC) functionals.[9] Even so, in many applications, it works well for low-lying valence states.[9] Considering large systems with a high density of excited states, it is not really necessary to describe individual excitations with high accuracy and a TD-DFT treatment including only singly-excited configurations might be sufficient.

A decade ago, the simplified time-dependent density functional theory (sTD-DFT) and its variant using the Tamm-Dancoff approximation (sTDA) were introduced by one of us[10,11]. These approaches were extended to range-separated hybrid (RSH) functionals by Risthaus et al.[12]. These methods were originally designed to evaluate ultra-violet/visible (UV/vis) and circular dichroism (CD) spectra of large molecules ($<$ 1000 atoms) for which it was not possible to use conventional TD-DFT. In 2016, these methods were extended to ultra-large systems with the extended tight-binding (xTB) variant[13], enabling the computation of excited states for organic systems up to 5000 atoms and more recently to compounds with 4d and 5d metals as well as 4p, 5p, and 6p elements.[14] Since then, the reach of these simplified QC (sQC) methods was expanded to response properties allowing the evaluation of the polarizability[15], optical rotation[16], excited state absorption[17], first hyperpolarizability[15], and two-photon absorption (2PA)[18]. A spin-flip variant[19] was also implemented as well as tools involving natural transition/response orbitals to interpret excited states[20] and response properties[21].

sTD-DFT/sTDA methods also inspired alternative schemes to speed-up excited state calculations. In 2016, Rüger et al.[22] proposed the TD-DFT+TB method. Also based on a DFT ground state, the TD-DFT+TB scheme uses a similar monopole approximation in the linear response treatment but considers local XC functionals instead of hybrid ones. Asadi-Aghbolaghi et al.[23] showed that the TD-DFT+TB method is up to 100× faster than TD-DFT to evaluate excited states of large gold and silver plasmonic nanoparticles with less than 0.15 eV of error with respect to TD-DFT for excitation energies. Recently, Havenridge et al.[24] extend this method to the efficient computation of the analytical excited state gradient using the Z-vector method. Giannone and Della Sala[25] proposed the TD-DFT-as method, TD-DFT using the resolution of identity (RI) with only one s-type Gaussian basis function per atom. The argued that sTD-DFT/sTDA/TD-DFT+TB can be seen as approximations to the TD-DFT-as method where three-index RI two-electron integrals are replaced by Löwdin approximated ones. The TD-DFT-as approach was recently extended to hybrid XC functionals with the TD-DFT-ris method[26]. The use of a minimal auxiliary basis set with TD-DFT reduced the cost by around two orders of magnitude while reproducing the full scheme exceptionally well. Hehn et al.[27] added periodic bondary conditions to the sTDA scheme by splitting the Coulomb operator into a semiempirical short-range and an exact long-range contribution. Simplified GW/Bethe-Salpether equation (BSE) were also proposed by Cho et al.[28] in 2022.

In a perspective article[29], we recently displayed future challenges for sQC methods. Among them, there was the idea to improve the global accuracy of sQC schemes by going beyond its monopole approximation to evaluate two-electron integrals. We explored this multipole approach but find an alternative route which is the subject of this work. The sTD-DFT/sTDA approximated molecular orbital (MO) two-electron integrals use atomic transition charges obtained from a Löwdin orthogonalization procedure and the Mataga-Nishimoto-Ohno-Klopman (MNOK)[30–32] damped Coulomb operator, a function of the interatomic distance. To recover this, instead of using the MNOK operator, Löwdin-orthogonalized two-electron integrals $(\lambda_\alpha\lambda_\alpha|\lambda_\beta\lambda_\beta)$ are approximated by atomic orbital (AO) two-electron integrals $(\alpha\alpha|\beta\beta)$. By removing the semi-empirical nature of the two-electron integrals, we arrive to an "ab initio" version of the sTD-DFT method where two-electron integrals in the zero differential overlap (ZDO) approximation[33] are computed exactly. This new method is introduced as the eXact integral simplified time-dependent density functional

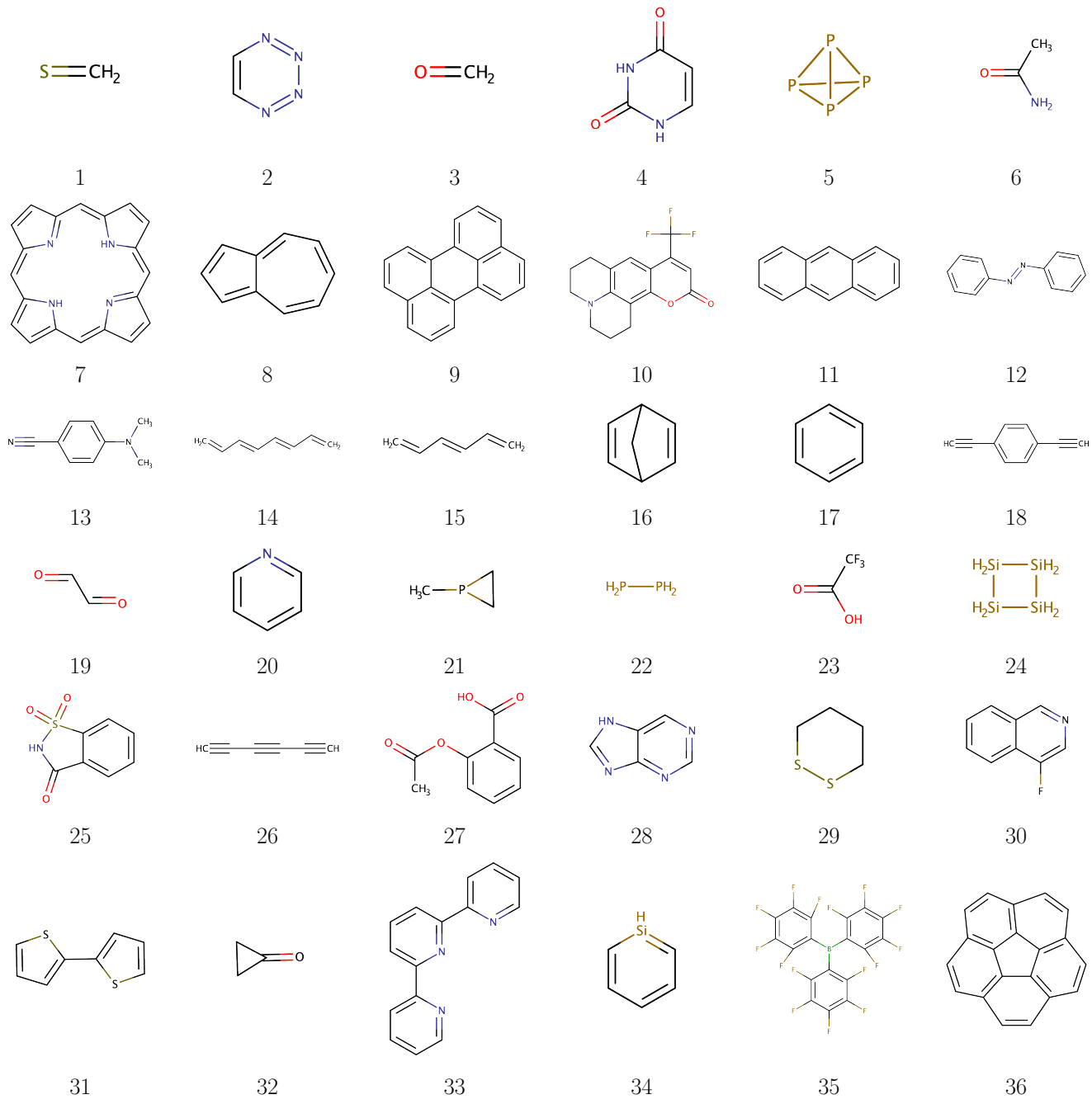

FIG. 1. Chemical structures of **1** to **36** from the benchmark set of 77 molecules (**1-17**[11], **18-20**[12], **21-46**[13], **47-57**[34], and **58-77**[12]).

theory (XsTD-DFT). Its TDA variant (XsTDA) is also presented.

To assess the performance of XsTDA for the evaluation of excited state energies and oscillator strengths, we benchmarked them with respect to TDA results for a set of 77 molecules taken from earlier works[11–13,34]. Figures 1 and 2 provide the chemical structures of these systems. Note that this set includes the DYE12 test set[34] which is composed of 12

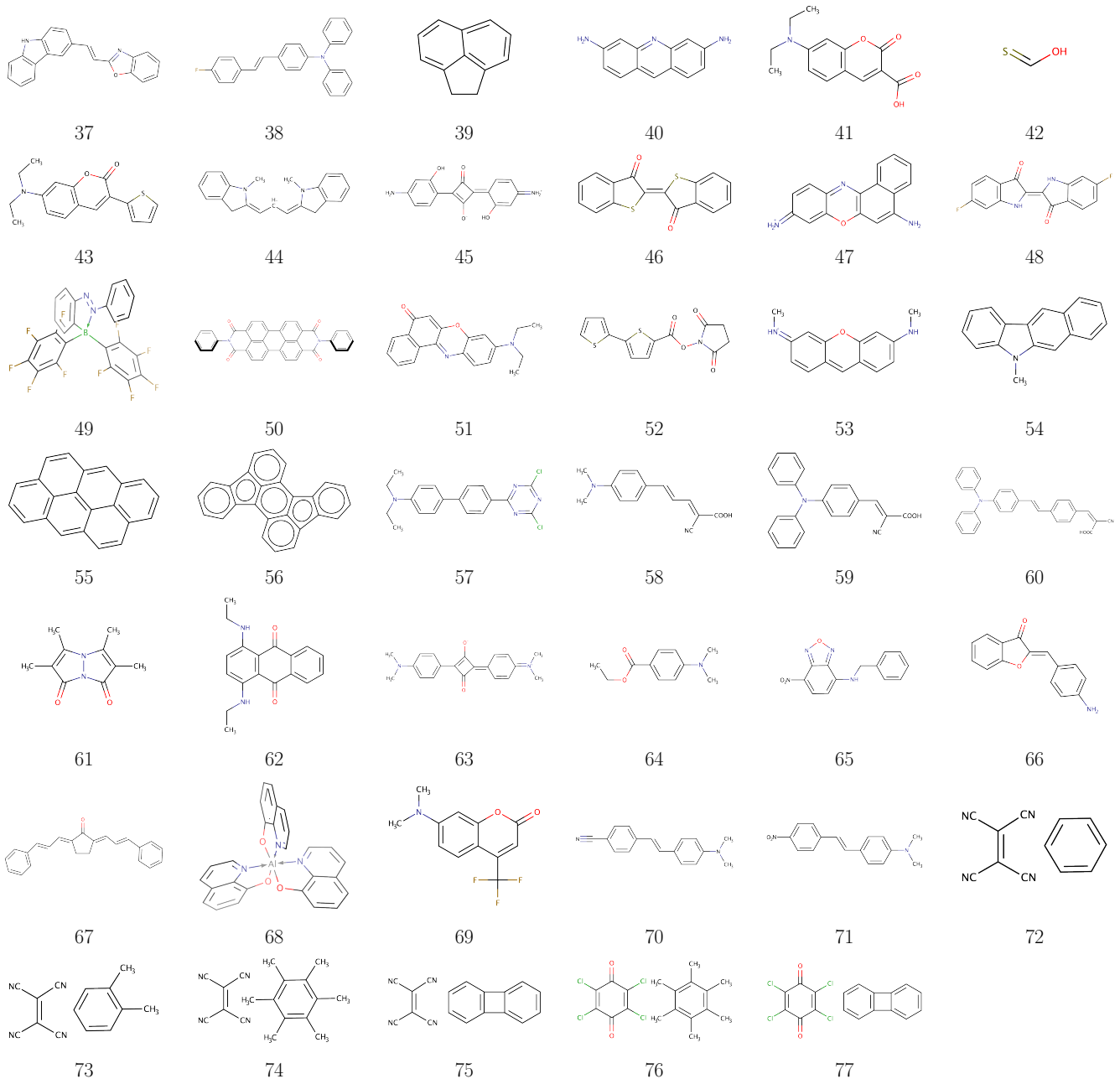

FIG. 2. Chemical structures of **37** to **77** from the benchmark set of 77 molecules (**1-17**[11], **18-20**[12], **21-46**[13], **47-57**[34], and **58-77**[12]).

large organic dyes and for which back-corrected "experimental" vertical excitation energies are available. This set also contains the mixed CT test set from Risthaus *et al.*[12] for which reference SCS-CC2/def2-TZVP(-f) excitation energies are available. In addition, UV/Vis. absorption spectra were computed and compared to experiment[35–37] for three anti-epileptic drugs: carbamazepine, lamotrigine, and diazepam.

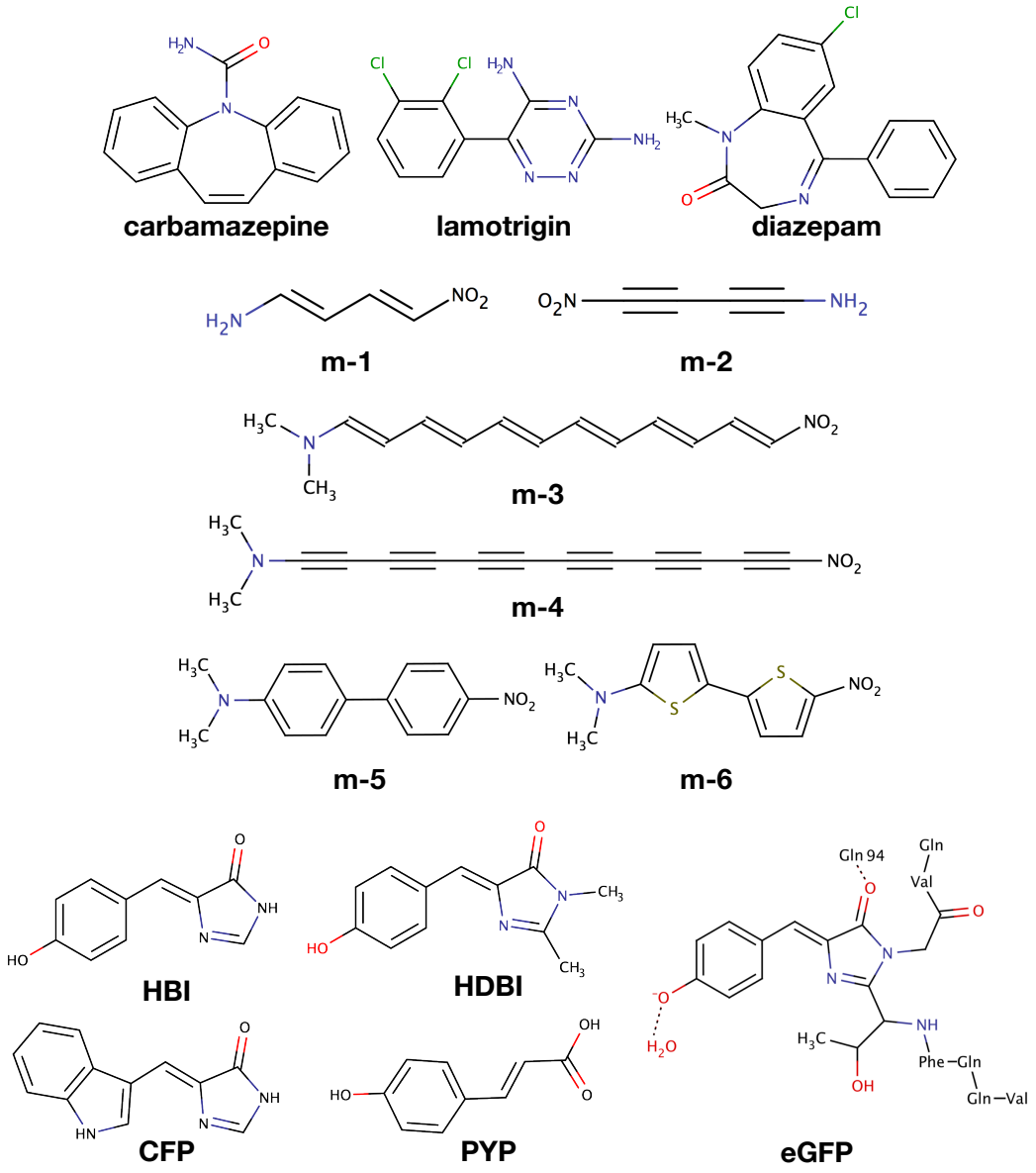

FIG. 3. Chemical structure of considered systems (except the benchmark set of 77 molecules): carbamazepine, lamotrigine, and diazepam, six push-pull π-conjugated molecules, four FP chromphores (HBI, HBDI, CFP, and PYP), and the eGFP chromophore with its first shell of residues.

The XsTD-DFT/XsTDA methods inherit from all previous implementations in the `stda` program[38]. Thus, this is the opportunity to benchmark nonlinear optical properties as well. To assess the performance of the XsTD-DFT method to compute the first hyperpolarizability, six push-pull π-conjugated molecules were employed to assess the performance of the XsTD-DFT method. Finally for 2PA, we looked at 2PA spectra for a set of fluorescent protein chromophores[39] and to the simulation of eGFP 2PA spectrum with a model structure

including eGFP chromophore and its first shell of surrounding residues[40]. Figure 3 presents these extra structures.

The article is organized as followed: first, we introduce the theoretical background for the XsTD-DFT/XsTDA methods for global hybrid XC functionals. Then, we provide computational details and discuss results before providing conclusions and outlooks.

II. THEORETICAL BACKGROUND

The XsTD-DFT/XsTDA methods are introduced by first recalling the density-matrix-based TD-DFT formalism[8,41–46] then showing how simplifications were originally applied to give rise to the sTD-DFT/sTDA framework[10,11,13,15–17,29] and finally how to remove its semi-empiricism. In the following, p, q, r, s indices refer to general molecular orbitals (MOs), i, j, k, l to occupied, a, b, c, d to unoccupied molecular orbitals, $\alpha, \beta, \gamma, \delta$ to atomic orbitals (AOs), and A, B to atoms. The Casida's TD-DFT equations[5] are usually used to compute excited states

$$\left[\begin{pmatrix} \mathbf{A} & \mathbf{B} \\ \mathbf{B} & \mathbf{A} \end{pmatrix} - \omega \begin{pmatrix} 1 & 0 \\ 0 & -1 \end{pmatrix}\right] \begin{pmatrix} \mathbf{X} \\ \mathbf{Y} \end{pmatrix} = 0 \tag{1}$$

or linear response properties in presence of a perturbation

$$\left[\begin{pmatrix} \mathbf{A} & \mathbf{B} \\ \mathbf{B} & \mathbf{A} \end{pmatrix} - \omega \begin{pmatrix} 1 & 0 \\ 0 & -1 \end{pmatrix}\right] \begin{pmatrix} \mathbf{X}_\zeta(\omega) \\ \mathbf{Y}_\zeta(\omega) \end{pmatrix} = - \begin{pmatrix} \mu_\zeta \\ \mu_\zeta \end{pmatrix}, \tag{2}$$

where X and Y are excitation and de-excitation vectors, respectively, $X_\zeta(\omega)$ and $Y_\zeta(\omega)$ frequency-dependent linear-response vectors, and a perturbation $\mu_{\zeta,ai} = \langle \phi_a | \hat{\mu}_\zeta | \phi_i \rangle$. Considering a hybrid exchange-correlation functional, $\mathbf{A}$ and $\mathbf{B}$ supermatrix elements are defined for a given amount a_x of Fock exchange as

$$A_{ia,jb} = \delta_{ij}\delta_{ab}(\epsilon_a - \epsilon_i) + 2(ia|jb) - a_x(ij|ab) + (1 - a_x)(ia|f_{XC}|jb) \tag{3}$$

and

$$B_{ia,jb} = 2(ia|bj) - a_x(ib|aj) + (1 - a_x)(ia|f_{XC}|bj), \tag{4}$$

where $(ia|jb)$, $(ia|bj)$, and $(ib|aj)$ are exchange-type and $(ij|ab)$ Coulomb-type two-electron integrals, $(ia|f_{XC}|jb)$ and $(ia|f_{XC}|bj)$ are the response of the exchange-correlation functional. To compute excited states using the Tamm-Dancoff approximation, the **B** supermatrix is neglected giving rise to a simple Hermitian eigenvalue problem

$$\mathbf{AX} = \omega\mathbf{X}. \tag{5}$$

The sTD-DFT/sTDA framework applied three approximations to these equations. First, terms involving the response of the exchange-correlation functional $(ia|f_{XC}|jb)$ and $(ia|f_{XC}|bj)$ are neglected in the expressions of **A** and **B** supermatrices. Second, the expansion space of configuration state functions (CSFs) is truncated considering a single cut-off energy E_{thresh}. In this procedure, the active MO space is determined for MO energies in between

$$\epsilon_{min} = \epsilon_{LUMO} - 2(1 + 0.8a_x)E_{thresh} \tag{6}$$

and

$$\epsilon_{max} = \epsilon_{HOMO} + 2(1 + 0.8a_x)E_{thresh}. \tag{7}$$

Then, the primary CSFs (P-CSFs) space is selected for $i \rightarrow a$ excitations when $A_{ia,ia} \leq E_{thresh}$. Remaining $j \rightarrow b$ excitations for which $A_{jb,jb} > E_{thresh}$ are only selected as secondary CSF (S-CSF) if

$$E_{jb}^{(2)} = \sum_{ia}^{P-CSFs} \frac{|A_{ia,jb}|^2}{A_{jb,jb} - A_{ia,ia}} > 10^{-4}E_h. \tag{8}$$

The full space of CSFs accounted for in the sTD-DFT/sTDA procedures for a given E_{thresh} is the sum of P-CSFs and S-CSFs. The last approximation regards two-electron integrals that are approximated by a monopole approximation to better balance cost and accuracy. MO two-electron integrals should be normally evaluated by the four-index transformation of AO two-electron integrals

$$(ia|jb) = \sum_{\alpha\beta\gamma\delta} C_{i\alpha}^* C_{a\beta} C_{j\gamma}^* C_{b\delta} \left(\alpha\beta|\gamma\delta\right). \tag{9}$$

This costly transformation is a computational bottleneck in conventional "ab initio" quantum chemistry. Considering an orthogonalized Löwdin basis $\lambda_\alpha = \sum_\beta \chi_\beta S_{\beta\alpha}^{-1/2}$, MO two-

electron integrals are equivalently computed as

$$(ia|jb) = \sum_{\alpha\beta\gamma\delta} C_{i\alpha}^{low*} C_{a\beta}^{low} C_{j\gamma}^{low*} C_{b\delta}^{low} \left(\lambda_\alpha \lambda_\beta | \lambda_\gamma \lambda_\delta\right). \tag{10}$$

Considering the ZDO approximation[33], MO two-electron integrals are approximated as

$$(ia|jb) \approx \sum_{\alpha\beta} C_{i\alpha}^{low*} C_{a\alpha}^{low} C_{j\beta}^{low*} C_{b\beta}^{low} \left(\lambda_\alpha \lambda_\alpha | \lambda_\beta \lambda_\beta\right). \tag{11}$$

Assuming that Löwdin-orthogonalized orbitals (LOs) are atom-centered and thus that Löwdin-orthogonalized coefficients do belong to a particular atom, transition charges can be collected for atom A as

$$Q_A^{ia} = \sum_{\alpha \in A} C_{\alpha i}^{low*} C_{\alpha a}^{low}. \tag{12}$$

The simplified expression for MO two-electron integrals reads

$$(ia|jb) \approx \sum_{AB} Q_A^{ia} Q_B^{jb} \left(AA|BB\right), \tag{13}$$

where

$$(AA|BB) = \sum_{\alpha \in A, \beta \in B} \left(\lambda_\alpha \lambda_\alpha | \lambda_\beta \lambda_\beta\right). \tag{14}$$

This expression implies that Löwdin-orthogonalized two-electron integrals can also be collected for atoms A and B. Equation 13 can be seen as a simple Coulomb law where $(AA|BB)$ is approximated by the MNOK[30–32] damped Coulomb operator that does not depend on LOs λ_α anymore.

For exchange integrals, it takes the form

$$(AA|BB)^K = \left(\frac{1}{(R_{AB})^{y_K} + \left(\frac{\eta_A + \eta_B}{2}\right)^{-y_K}} \right)^{\frac{1}{y_K}}, \tag{15}$$

while for Coulomb integrals, it reads

$$a_x \left(AA|BB\right)^J = \left(\frac{1}{(R_{AB})^{y_J} + \left(a_x \frac{\eta_A + \eta_B}{2}\right)^{-y_J}} \right)^{\frac{1}{y_J}}, \tag{16}$$

where y_K and y_J are globally-fitted parameters for the whole range of a_x, R_{AB} is the interatomic distance, and η_A is the chemical hardness of atom A. This also means that the onsite integral $(AA|AA)$ is simply the chemical hardness η_A of A multiplied or not by a_x considering the type of integrals. The MNOK approximation eliminates the dependence on LOs of equation 14. These expressions are quite beneficial in terms of computational costs by first pre-computing

$$(ia|BB) = \sum_A Q_A^{ia} \, (AA|BB) \tag{17}$$

and then taking the dot product that scale with the number of atoms when constructing $\mathbf{A}$ and $\mathbf{B}$ supermatrices

$$(ia|jb) \approx \sum_B (ia|BB) \, Q_B^{jb}. \tag{18}$$

This constitutes the basis of sTD-DFT/sTDA schemes.

Now, we introduce the XsTD-DFT/XsTDA methods. It is common in semi-empirical molecular orbital models[47] to replace Löwdin-orthogonalized two-electron integrals by AO ones according to

$$(ia|jb) \approx \sum_{\alpha\beta} C_{i\alpha}^{low*} C_{a\alpha}^{low} C_{j\beta}^{low*} C_{b\beta}^{low} \, (\alpha\alpha|\beta\beta) \, . \tag{19}$$

Thus, AO transition charges can be collected for each basis functions as

$$Q_\alpha^{ia} = \sum_\alpha C_{\alpha i}^{low*} C_{\alpha a}^{low} \, . \tag{20}$$

Expression 19 becomes

$$(ia|jb) \approx \sum_{\alpha\beta} Q_\alpha^{ia} Q_\beta^{jb} \, (\alpha\alpha|\beta\beta) \, . \tag{21}$$

In the same way as in sTD-DFT/sTDA schemes, its evaluation becomes computationally efficient by pre-computing

$$(ia|\beta\beta) = \sum_\alpha Q_\alpha^{ia} \, (\alpha\alpha|\beta\beta) \tag{22}$$

and then taking the dot product that scales with the number of AOs

$$(ia|jb) \approx \sum_\beta (ia|\beta\beta) \, Q_\beta^{jb}. \tag{23}$$

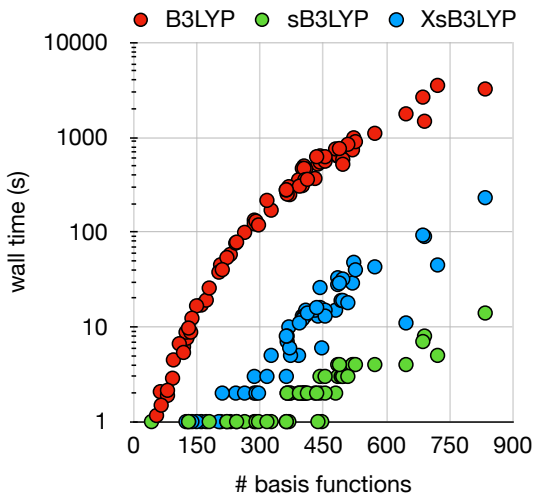

FIG. 4. B3LYP, sB3LYP, XsB3LYP computation wall times as a function of the number of basis functions for the set of 77 molecules. TDA calculations computed 20 excited states while sTDA and XsTDA ones considered $E_{thresh.} = 10$ eV.

In XsTD-DFT/XsTDA, we still consider the original three simplifications of the sTD-DFT method but two-electron integrals to generate **A** and **B** supermatrices are now computed using one- and two-center AO two-electron integrals with equation 23. Thus, we removed the 'semiempirical' nature of sTD-DFT/sTDA methods.

Note that in our implementation the CSFs space is still determined with the MNOK integrals for efficiency without any noticeable changes in the results. Compared to the sTD-DFT scheme, the XsTD-DFT is computationally more involved because computation times to construct **A** and **B** supermatrices scale with the number of AOs rather than the number of atoms. Figure 4 presents computation wall times as a function of the number of basis functions to compute the 20 first excited states for the benchmark set of 77 molecules (Fig. 1 and 2) at the B3LYP/6-31+G(d) level of theory on 8 CPUs (Intel Xeon CPU E5-2660 v4, 3.2 GHz). Wall times are also reported for sB3LYP and XsB3LYP calculations considering $E_{thresh.} = 10$ eV performed on a 8 core desktop computer (Intel core i7-6700, 3.4 GHz). Usually when considering $E_{thresh.} = 10$ eV, more than 1000 excited states are computed for these systems. Note that the number of excited states computed depends on the system and $E_{thresh.}$. Thus, it is not possible to give formal scaling factors for simplified methods. For molecule **50**, 1204 and 1121 states were computed at both sB3LYP and XsB3LYP levels of theory in 14 s and 3.85 min, respectively. The full TD-DFT calculation took 26.50 min. Using a smaller $E_{thresh.}$ value of 7 eV (`stda` program[38] default), the XsTDA calculation

computed "only" 223 excited states in 23 s. This is more than 60 time faster with respect to the full scheme. For compound **35**, the TDA calculation took 25.5 min while sTDA and XsTDA ones ($E_{thresh.}$ = 10 eV) only 4 and 11 s, respectively. This is 382 and 139 time faster. For this benchmark set, considering $E_{thresh.}$ = 10 eV, the average speed-up is around 100 for sTDA and 20 for XsTDA. These factors can be increased by using a smaller $E_{thresh.}$ value.

III. COMPUTATIONAL DETAILS

The XsTD-DFT/XsTDA methods were implemented in a development version of the freely-available `stda` program[38] that is now interfaced with the Libcint library[48] to allow the computation of AO two-electron integrals. This implementation benefits from the whole range of linear and nonlinear optical properties already implemented at the sTD-DFT/sTDA levels of theory in the `stda` program[38] including UV/vis absorption[10,11], CD[10,11], polarizability[15], optical rotation[16], excited state absorption[17], first hyperpolarizability[15], and two-photon absorption[18].

To test the performance of the XsTDA method to compute excited state energies and oscillator strengths, a set of 77 molecules (Fig. 1 and 2) was constituted from previous works[11–13,34]. Optimized structures of **1-17** were taken from Bannwarth and Grimme[11], **18-20** and **58-77** from Risthaus et al.[12], **21-46** from Grimme and Bannwarth[13], and **47-57** from Goerigk and Grimme[34]. Note that this set of molecules includes the DYE12 test set that was used to assess the treatment of low-lying valence excitations of large organic dyes.[34] Geometries **10** and **47-57** belong to that test set. Back-corrected "experimental" vertical excitation energies are also taken from reference 34. Molecules **69-77** are parts of the mixed CT test set[12] for which reference excitation energies for transitions to CT states are available at the SCS-CC2/def2-TZVP(-f) level of theory. Additional RI-CC2/aug-cc-pVDZ excitation energies were computed for **72** for different distances between benzene and TCNE molecular plans.

To assess the performance of the XsTDA method to compute UV/Vis absorption spectra, we first compare it to the experimental spectrum of the largest molecule of the benchmark set of 77 molecules, i.e., molecule **50** (perylene-3,4,9,10-tetracarboxylic bisimide) that was taken from Langhals[49]. Second, the structure of ferrocene was optimized at the ωB97X-D3/def2-

TZVP level of theory. Its experimental absorption spectrum was taken from reference 10 for comparison. Third, we selected three drugs: carbamazepine, lamotrigine, and diazepam for which their structures were optimized at the ωB97X-D3/6-311G(d) level of theory. Experimental UV/vis absorption spectra were taken from references 35, 36, and 37, respectivelly.

Reference TD-DFT/TDA excited state calculations were performed with Q-CHEM[50] using B3LYP, PBE0, BHandHLYP, and M06-2X functionals and the 6-31+G(d) basis set for the set of 77 molecules. BHandHLYP/6-31+G(d) TD-DFT/TDA calculations were also performed with Q-CHEM[50] for carbamazepine, lamotrigine, and diazepam while sTDA and XsTDA computations employed the same functional/basis set combination. For the set of 77 molecules, an energy threshold of 10 eV was employed to truncate the CSFs space while the default value of 7 eV was used for other compounds. For ferrocene, the 20 first excited states were computed at the PBE0/def2-TZVP/TD-DFT/TDA level of theory and compared to sTDA and XsTDA results using $E_{thresh.} = 7$ eV. Note that to simulate intensity borrowing by vibronic coupling, forbidden transition oscillator strengths were set to 5×10^{-4} as it was originally proposed by one of us[10].

To assess the performance of the XsTD-DFT method to reproduce frequency-dependent hyper-Rayleigh scattering first hyperpolarizability (β_{HRS}) values, the structures of six push-pull π-conjugated molecules that were originally used to benchmarked the sTD-DFT method[15] were taken from de Wergifosse and Champagne[40]. TD-DFT and sTD-DFT BHandHLYP/6-31+G(d) β_{HRS} frequency dispersions were taken from de Wergifosse et al.[15]. XsTD-DFT β_{HRS} values were computed at the same level.

For 2PA, we first used the same set of FP chromophores that we employed to benchmark the sTD-DFT method.[18] These structures were taken from from reference 39 as well as reference excitation energies and 2PA cross-sections (σ_{2PA}) at the RI-CC2/d-aug(-d)-cc-pVDZ level for HBI, HBDI, and PYP and with the aug-cc-pVDZ basis set for CFP as well as EOM-CCSD/d-aug(-d)-cc-pVDZ level[51], when available. Second, we took eGFP chromophore and its first shell of surrounding residues from de Wergifosse et al.[52]. This structure was successfully-used to evaluate the 2PA of eGFP at the sTD-DFT-xTB level of theory.[18] The experimental 2PA spectrum was recorded by Drobizhev et al.[53] Regarding FP chromophores, TD-DFT 2PA cross-sections and excited state energies were computed using Dalton2018.0[54,55] with the 6-31+G(d) basis set and B3LYP. sTD-DFT and XsTD-DFT calculations were performed with the same XC functionals and basis set. For eGFP,

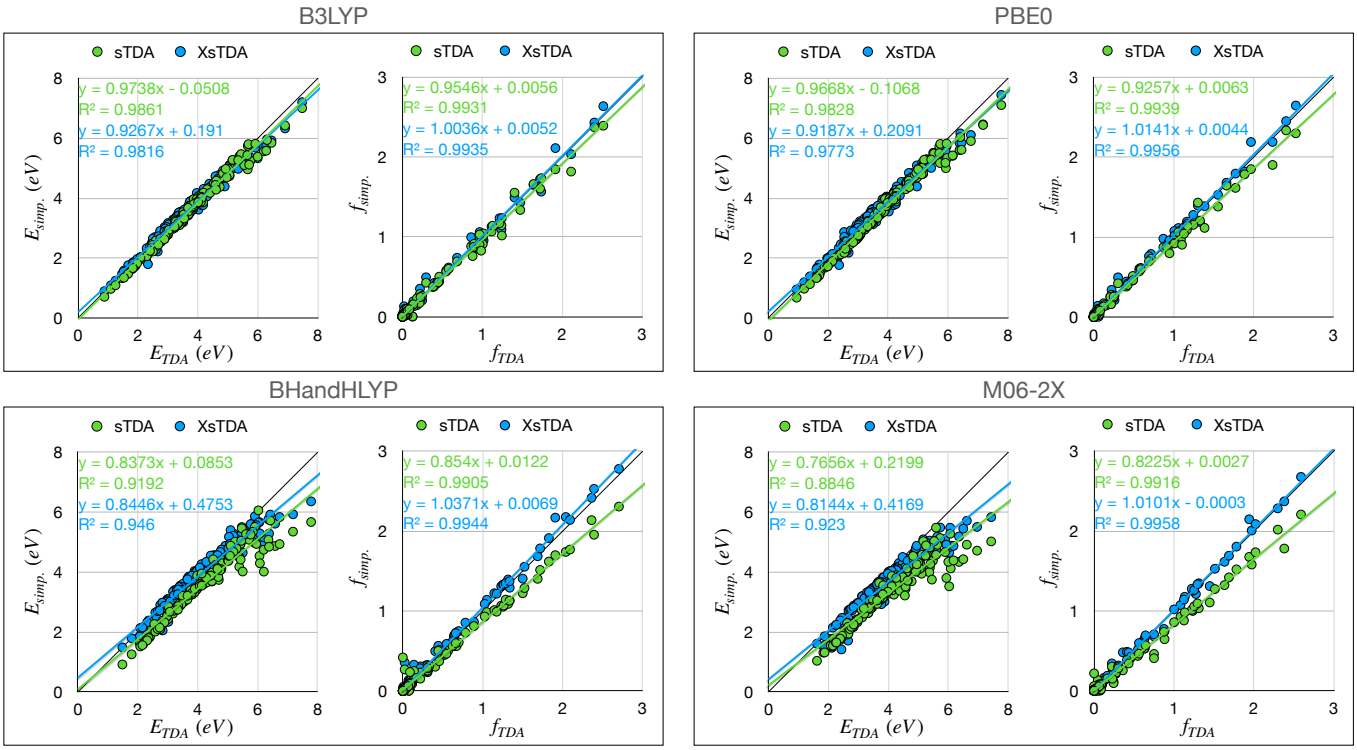

FIG. 5. For the two lowest-lying singlet excited states of the set of 77 molecules, correlation graphs for sTDA and XsTDA excitation energies with respect to TDA ones as well as for oscillator strengths using B3LYP, PBE0, BHandHLYP, and M06-2X exchange-correlation functionals and the 6-31+G(d) basis set. Linear regression data are also provided.

the B3LYP/6-31G(d) calculations were performed at both sTD-DFT and XsTD-DFT levels of theory.

Input molecular orbitals and their energies for the sTD-DFT and XsTD-DFT calculations used by the `stda` program[38] were computed with Q-Chem 5.1[50]. All geometry optimizations were also performed with Q-Chem[50]. RI-CC2 excitation energies were computed with Turbomole 7.6[56]. β_{HRS} values are given in atomic units considering the Taylor series convention[57] while 2PA strengths $\langle \delta^{2PA} \rangle$ are in a.u. and σ_{2PA} in GM (Göppert-Mayer) units.

IV. RESULTS AND DISCUSSIONS

A. Excitation energies, oscillator strengths, and UV-vis spectra

Figure 5 presents excitation energy and oscillator strength correlation plots for the two lowest-lying singlet excited states of the set of 77 molecules for sTDA and XsTDA with

E (eV)	**sB3LYP**	**XsB3LYP**	**sPBE0**	**XsPBE0**	**sBHandHLYP**	**XsBHandHLYP**	**sM06-2X**	**XsM06-2X**
MAD	0.16	0.14	0.24	0.16	0.61	0.24	0.74	0.35
max AD - min AD	0.70	0.70	0.92	0.74	2.18	1.42	2.45	1.60
MD	-0.15	-0.08	-0.24	-0.10	-0.60	-0.18	-0.74	-0.35
f $\in [0.0; 0.1[$	**sB3LYP**	**XsB3LYP**	**sPBE0**	**XsPBE0**	**sBHandHLYP**	**XsBHandHLYP**	**sM06-2X**	**XsM06-2X**
MAD	0.01	0.01	0.01	0.01	0.01	0.01	0.01	0.01
max AD - min AD	0.06	0.11	-0.05	-0.08	0.42	0.33	0.22	0.07
MD	+0.00	+0.00	+0.00	+0.00	+0.01	+0.00	+0.00	0.00
f $\in [0.1; 1.0[$	**sB3LYP**	**XsB3LYP**	**sPBE0**	**XsPBE0**	**sBHandHLYP**	**XsBHandHLYP**	**sM06-2X**	**XsM06-2X**
MAD	0.04	0.05	0.03	0.04	0.05	0.05	0.10	0.06
max AD - min AD	0.15	0.19	0.15	0.19	0.11	0.19	0.34	0.14
MD	-0.01	+0.02	-0.01	+0.03	+0.07	+0.03	-0.09	-0.00
f $\in [1.0; 3.0]$	**sB3LYP**	**XsB3LYP**	**sPBE0**	**XsPBE0**	**sBHandHLYP**	**XsBHandHLYP**	**sM06-2X**	**XsM06-2X**
MAD	0.09	0.06	0.12	0.05	0.22	0.08	0.27	0.04
max AD - min AD	0.29	0.20	0.33	0.22	0.37	0.26	0.46	0.20
MD	-0.07	-0.00	-0.11	+0.02	-0.22	+0.07	-0.27	+0.02

TABLE I. For B3LYP, PBE0, BHandHLYP, and M06-2X exchange-correlation functionals, mean absolute deviations (MAD), difference between maximum and minimum absolute deviations (AD), and mean deviations (MD) among the set of 77 molecules for sTDA and XsTDA excitation energies and oscillator strengths with respect to TDA ones. The sign of MD indicates a systematic overestimation or underestimation.

respect to TDA using B3LYP, PBE0, BHandHLYP, and M06-2X XC functionals. For each functionals, table I provides statistical analysis of the excitation energies and oscillator strengths considering regular TDA results as the reference. For oscillator strengths, statistical analysis are given by orders of magnitude (f $\in$ [0.0;0.1[, [0.1;1.0[, and [1.0;3.0]). Note that the first range of magnitude includes the order from 0.01 to 0.1 but also lower oscillator strengths for convenience. The statistical analysis includes mean absolute deviations (MAD), differences between maximum and minimum absolute deviations (AD) representing the error spread, and mean deviations (MD) for which the sign can indicate systematic overestimation or underestimation.

For B3LYP, both sTDA and XsTDA excitation energies deviate only slightly with respect to TDA ones with MAD values of 0.16 and 0.14 eV for sTDA and XsTDA, respectively. This shows that the sTDA method is particularly well parameterized for small amounts of Fock exchange. The error spreads have the same order of magnitude for both methods. Oscillator strength MADs are small for their respective ranges of magnitude with both methods. The XsB3LYP scheme slightly outperforms sB3LYP for oscillator strengths larger or equal to 1.0 with respect to B3LYP results. This is confirmed by the correlation graph (Figure 5).

Considering PBE0 with a 25% Fock exchange contribution, the MAD is increased to 0.24 eV for sTDA while it remains almost constant for XsTDA with 0.16 eV. Increasing the amount of Fock exchange in the functional globally increases the MAD for the sTDA scheme as confirmed by sBHandHLYP and sM06-2X results. Excitation energy deviations remain smaller with the XsTDA scheme than for the sTDA one. The sM06-2X MAD of 0.74 eV is more than two times larger than the XsM06-2X MAD of 0.35 eV. Similar trends are observed for oscillator strengths especially in the [1.0;3.0] range for which the XsTDA method clearly outperforms the sTDA approach (Figure 5). Perylene (**9**) was one of the sTDA "outliers" pointed out by Grimme[10] with an absolute energy deviation larger than 0.50 eV at the sPBE0/TZVP level with respect to experiment. For the first low lying excited state of perylene, the TDA/PBE0/6-31+G(d) excitation energy is 0.37 eV smaller than the experimental value of 3.44 eV while the XsPBE0 value is -0.27 eV away. This is a large improvement with respect to the sTDA absolute deviation of 0.60 eV.

Figure 6 presents sTDA and XsTDA excitation energy absolute deviations with respect to regular TDA as a function of the number of electrons in the molecule. Considering all four functionals, ADs are diminishing when increasing number of electrons for both sTDA and XsTDA with respect to TDA. ADs are globally lower for large systems when using the XsTDA method rather than the sTDA one. This supports the suitability of the XsTDA scheme to compute excitation energies for low lying excited states of large systems.

The DYE12 test set comprises 12 large organic dyes (**10** and **47-57**) for which back-corrected "experimental" vertical excitation energies in gas phase were obtained by Goerigk and Grimme[34]. For the DYE12 benchmark set, table S1 and S2 compare computed sTDA and XsTDA excitation energies to TDA as well as to the back-corrected experiment. The XsTDA method reproduced very well TDA excitation energies with MADs of about 0.10 eV. With respect to the back-corrected experiment, the best result is provided by the XsB3LYP scheme with a MAD of 0.23 eV while TDA results are close with a MAD of 0.24 eV. Note that the best sTDA comparison with respect to experiment is obtained with the BHandHLYP functional with a MAD of 0.23 eV. Clearly, the sTDA parametrization and error cancellations plays a large role in this result because the TDA MAD is 0.37 eV with respect to experiment.

Compound **50** is the largest molecule from this benchmark set with 246 electrons and 834 basis functions (6-31+G(d)). Figure 7 presents the experimental absorption spectrum of molecule **50** recorded by Langhals[49] that was back-corrected with the same shift as its

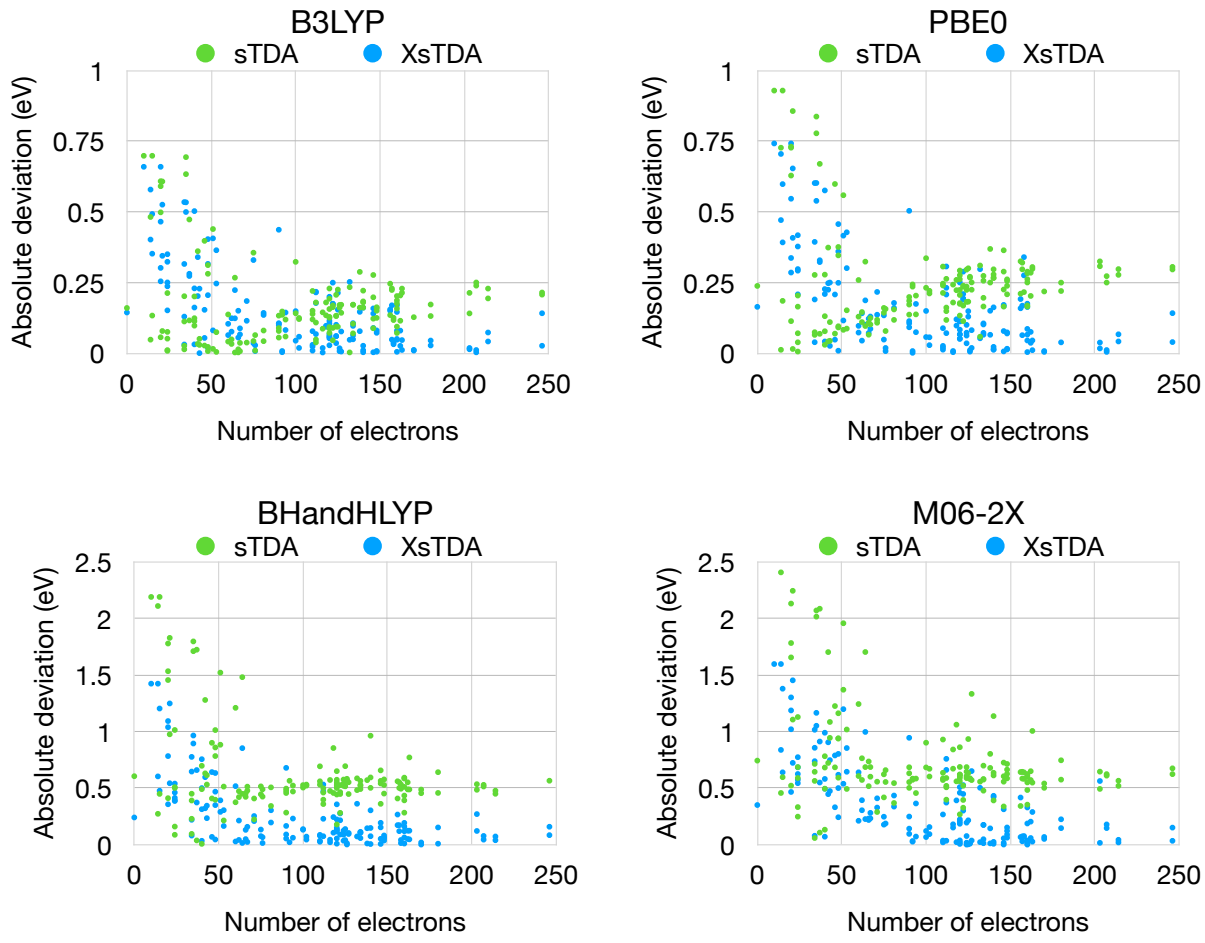

FIG. 6. Excitation energy absolute deviations of both sTDA and XsTDA methods with respect to TDA calculations as a function of the number of electrons for B3LYP, PBE0, BHandHLYP, and M06-2X functionals for the set of 77 molecules.

excitation energy from the DYE12, i.e., +0.35 eV (including +0.24 eV for the adiabatic energy and +0.11 eV to remove solvent effects). The normalized back-corrected experimental spectrum is compared to B3LYP/6-31+G(d) TDA, sTDA, and XsTDA ones. Note, that our calculations cannot account for the experimentally observed vibronic structure. The XsB3LYP spectrum provides an excellent comparison with experiment while B3LYP and sB3LYP ones are red-shifted by 0.12 and 0.34 eV, respectively.

As originally pointed out by one of us[10], while $\pi \rightarrow \pi^*$ transitions are relatively well-treated by the sTDA scheme, larger discrepancies were observed regarding $n \rightarrow \pi^*$ and $d \rightarrow d$ transitions due to the applied monopole approximation. To illustrate this behavior and how the XsTDA scheme deals with these types of excitations, we first selected uracil (**4**) that presents a dipole-forbidden $n \rightarrow \pi^*$ excitation and a $\pi \rightarrow \pi^*$ transition as the two first

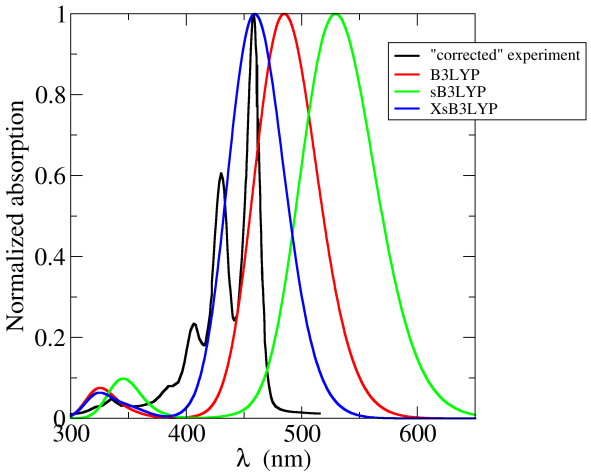

FIG. 7. Normalized back-corrected experimental UV-vis. spectrum (+0.35 eV) of **50** as well B3LYP/6-31+G(d) TDA, sTDA, and XsTDA ones.

Uracil	TDA			sTDA			XsTDA		
	ΔE (eV)	f	transition	ΔE (eV)	f	transition	ΔE (eV)	f	transition
1	5.38	0.00	$n \rightarrow \pi^*$	4.52	0.00	$\pi \rightarrow Ry$	5.03	0.00	$n \rightarrow \pi^*$
2	5.91	0.29	$\pi \rightarrow \pi^*$	5.19	0.00	$n \rightarrow \pi^*$	5.36	0.01	$\pi \rightarrow Ry$
3				5.40	0.00	$\pi \rightarrow Ry$	5.86	0.32	$\pi \rightarrow \pi^*$
4				5.51	0.24	$\pi \rightarrow \pi^*$			

TABLE II. Excitation energies (eV), oscillator strengths, and types of transition for the two lowest-lying singlet excited states of uracil obtained with BHandHLYP/6-31+G(d) TDA, sTDA, and XsTDA schemes.

low-lying singlet excited states. Table II presents the excited state energies and oscillator strengths as obtained by BHandHLYP/6-31+G(d) TDA, sTDA, and XsTDA schemes. First, both sTDA and XsTDA schemes yield $\pi \rightarrow Ry$ unwanted low-lying "ghost" states that are not present in the TDA calculation. Second, the $\pi \rightarrow \pi^*$ transition is better treated by the XsTDA method with only -0.05 eV of deviation with respect to the full scheme while the sTDA errors is -0.40 eV. For, the $n \rightarrow \pi^*$ transition, relatively large deviations are observed with both sTDA and XsTDA schemes (-0.19 and -0.35 eV). As stressed out by one of us[10], $n \rightarrow \pi^*$ transition are badly described by sTD-DFT/sTDA because of wrong localized exchange-type contributions due to the monopole approximation. This is inherent to any ZDO-based methods such as the XsTD-DFT/XsTDA formalism since one-center exchange integrals $[(\alpha\beta|\alpha\beta)$, α and $\beta \in A]$ are simply excluded.[58] Thus, the

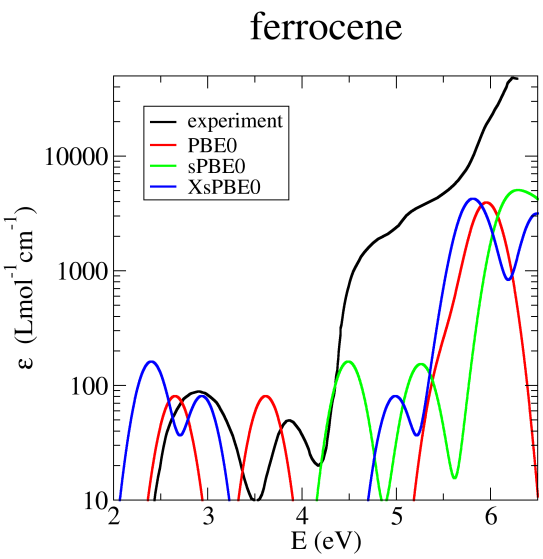

FIG. 8. Experimental absorption spectrum of ferrocene in comparison with PBE0/def2-TZVP TDA, sTDA, and XsTDA spectra. Note that oscillator strengths for forbidden transitions are set to 5×10^{-4} to simulate vibronic couplings.

XsTD-DFT/XsTDA formalism presents the same problem as the sTD-DFT/sTDA scheme to describe local $n \rightarrow \pi^*$ transitions. A possible correction could be to use the INDO (intermediate neglect of differential overlap) approximation[59] instead of the ZDO one.

As a second illustrative case, we selected the ferrocene molecule that was already used in the original sTDA publication[10] to illustrate the relative poor treatment of $d \rightarrow d$ transitions by the sTDA method. Figure 8 shows the experimental absorption spectrum of ferrocene in comparison with PBE0/def2-TZVP TDA, sTDA, and XsTDA spectra. The experimental spectrum presents three main absorption bands where the two lowest ones are related to dipole-forbidden metal-centered $d \rightarrow d$ transitions. These two bands are poorly described by the sTDA method which are significantly improved with the XsTDA scheme. The rest of the XsTDA spectrum is globally blue-shifted with respect to the experiment.

Treating correctly electronic transitions to Rydberg states is probably out of the scope of XsTD-DFT/XsTDA schemes. Nevertheless, among the test set, we have the first one photon-active transition $n \rightarrow Ry(3s)$ of acetone (**3**) with an experimental excitation energy of 6.35 eV and a reference theoretical oscillator strength of 0.037 (MRCI[1]). At the B3LYP/6-31+G(d) level, the experimental excitation energy is largely overestimated with a value of 6.91 eV but the MRCI oscillator strength is well reproduced with a value of 0.035. Only

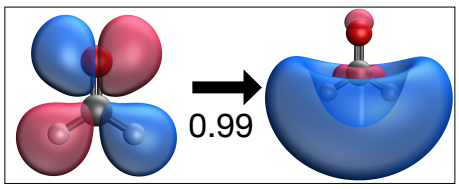

FIG. 9. Natural transition orbitals obtained at the TDA/B3LYP/6-31+G(d) level of theory for the first one photon active electronic transition of acetone. Only one pair contributes to the transition with a weight of 0.99.

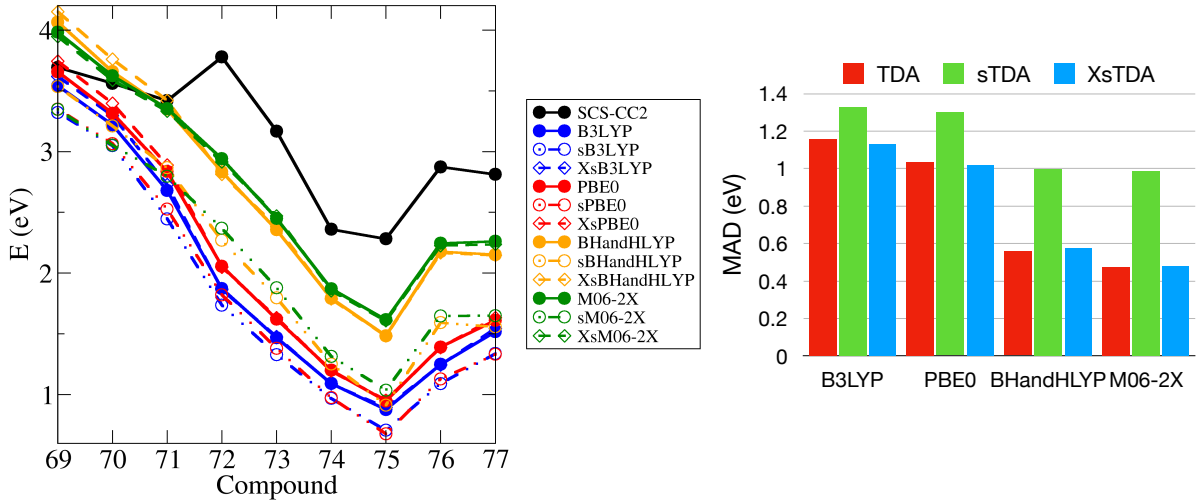

FIG. 10. Excitation energies (left panel) computed at TDA, sTDA, and XsTDA levels using B3LYP, PBE0, BHandHLYP, and M06-2X exchange-correlation functionals and 6-31+G(d) basis set in comparison with reference SCS-CC2/def2-TZVP(-f) values for the mixed CT test set[12]. Mean absolute deviations (right panel) for all these levels of theory with respect to SCS-CC2.

one pair of natural transition orbitals (NTOs) contributes to this transition, confirming its $n \rightarrow Ry(3s)$ character (Fig. 9, note that the $Ry(3s)$ extend of the electron NTO is more prominent with a smaller isovalue). The treatment is surprisingly improved with the XsB3LYP scheme giving an excitation energy of 6.33 eV and f =0.037. The shape of NTOs at this level are similar to B3LYP ones. The sB3LYP level of theory is also providing a better energy value with respect to the full scheme with 6.46 eV (f =0.035).

Hybrid XC functionals do not provide a good description for electron transitions to CT states. Usually, increasing the amount of Fock exchange into the functionals improves the treatment but still large deviations are observed.[10,60] Employing range-separated hybrid functionals is the usual solution for a better treatment of CT states but is not yet implemented with XsTD-DFT/XsTDA schemes. To assess the performance of the XsTDA scheme

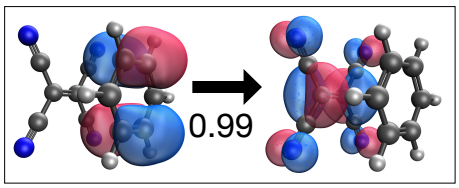

FIG. 11. Natural transition orbitals obtained at the TDA/BHandHLYP/6-31+G(d) level of theory for the first low-lying state of system **72**. Only one pair contributes to the transition with a weight of 0.99.

to treat CT states, the mixed CT test set from Risthaus *et al.*[12] was selected to provide an overview of its abilities using hybrid XC functionals. Figure 10 presents the comparison between TDA, sTDA, and XsTDA excitation energies to CT states using B3LYP, PBE0, BHandHLYP, and M06-2X exchange-correlation functionals and 6-31+G(d) basis set and reference SCS-CC2/def2-TZVP(-f) values. MADs for these excitation energies with respect to SCS-CC2 are also reported. As expected, XC functional with large amount of HF exchange compare the best with the reference. MADs for BHandHLYP and M06-2X are 0.56 and 0.48 eV respectively. XsTDA almost perfectly reproduces TDA results while sTDA on the contrary presents larger MADs with respect to the reference (MAD(sBHandHLYP) = 1.00 eV and MAD(sM06-2X) = 0.98 eV). Regarding intermolecular CT states from systems **72-77**, all reference excitation energies are systematically underestimated by TDA, a behavior almost perfectly reproduced by the XsTDA scheme.

72 is composed of one benzene and one TCNE units for which their molecular plans are parallel to each other. Figure 12 presents the first low-lying excited state energy of this system (see Fig. 11 for NTOs) as a function the distance (R) between both molecular plans evaluated at the TDA, sTDA, and XsTDA (BHandHLYP/6-31+G(d)) levels of theory with respect to the reference RI-CC2/aug-cc-pVDZ. A reference curve is also provided and computed as $E_{CT} = IP' - EA' - 1/R$ where IP' is the KS-DFT HOMO energy of benzene and EA', the KS-DFT LUMO energy of TCNE. All TDA, sTDA, and XsTDA results tends asymptotically to an excitation energy value around 1.28 eV lower than the RI-CC2 one. This was expected for hybrid XC functionals because of the integer discontinuity problem and the self-interaction error.[10,61–63] At large distance, this CT state is composed of benzene$^+$ and TCNE$^-$, two charges with a $1/R$ interaction energy. In TD-DFT, this interaction is translated by the $-(ii|aa)$ term in equation 1 but scaled by a_x. Because of this, it does not give the expected $1/R$ decay. By design the sTDA scheme was corrected for this behavior by

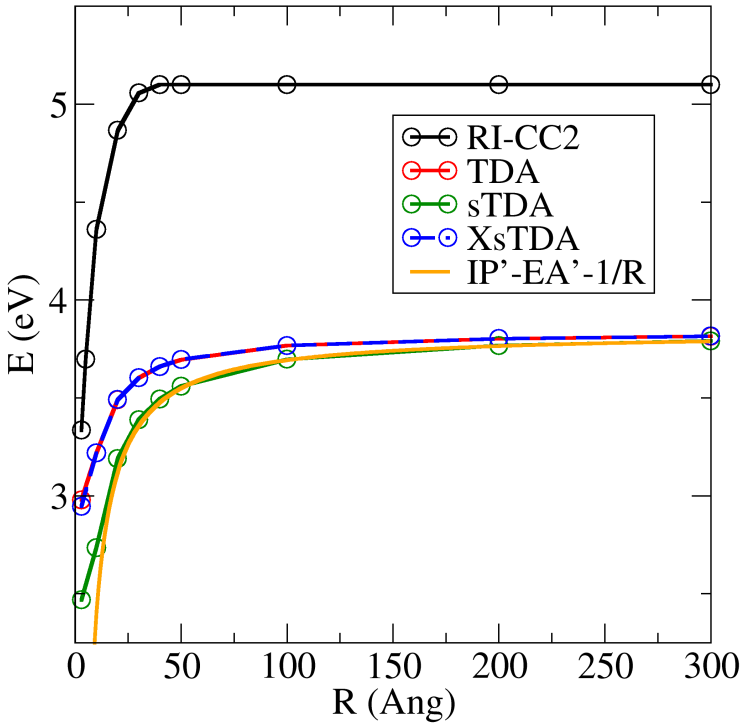

FIG. 12. Comparison of CT excitation energies computed at TDA, sTDA, and XsTDA (BHandHLYP/6-31+G(d)) levels of theory with respect to RI-CC2/aug-cc-pVDZ reference for molecule **72** as a function of the distance (R) between both parallel molecular plan of benzene and TCNE. A reference analytical single-particle curve is also provided.

asymptotically approaching the $1/R$ contribution directly into the semi-empirical integral (see eq.16).[10] This is illustrated in Figure 12 showing that the sTDA scheme reproduces well the $E_{CT} = IP' - EA' - 1/R$ curve while the XsTDA scheme matches almost perfectly the TDA results. These results on CT excited states illustrate the robustness of the XsTDA scheme to reproduce TDA excitation energies for this kind of states.

Figure 13 presents experimental absorption spectra[35–37] of three anti-epileptic drugs carbamazepine, lamotrigine, and diazepam recorded in methanol for the carbamazepine and in water for lamotrigine and diazepam. They are compared to BHandHLYP/6-31+G(d) TDA, sTDA, and XsTDA spectra. As it was observed for the benchmark set, sBHandHLYP/TDA excitation energies are red-shifted with respect to BHandHLYP/TDA ones. This behavior is corrected when employing the XsTDA scheme instead. In that case, TDA spectra are

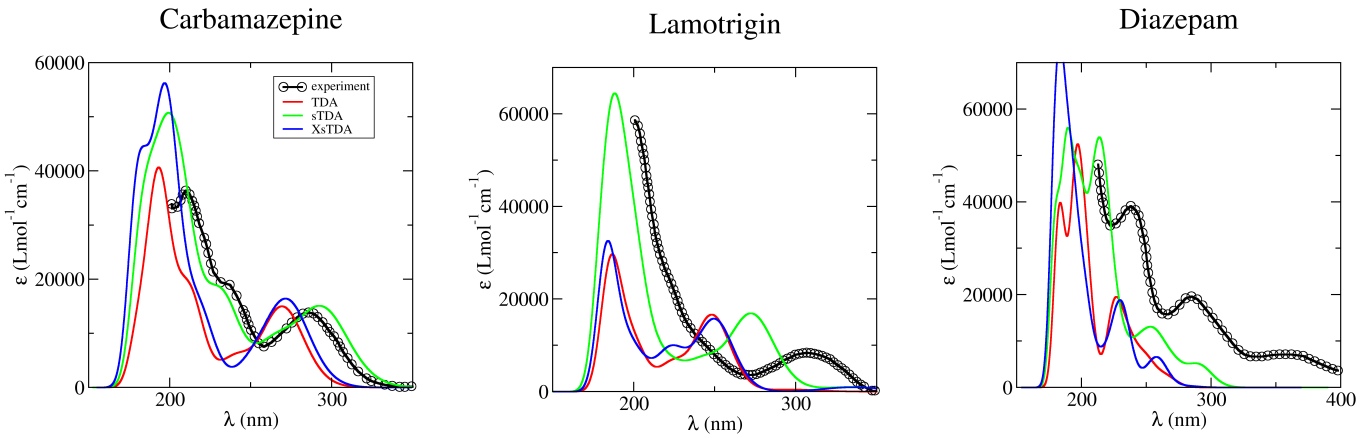

FIG. 13. UV-vis experimental absorption spectra[35–37] of carbamazepine in methanol, lamotrigine and diazepam in water as well as BHandHLYP/6-31+G(d) TDA, sTDA, and XsTDA spectra in vacuum.

well reproduced. TDA and XsTDA spectra are systematically blue-shifted with respect to experiment because of missing solvent, relaxation and vibrational effects. Note that in the case of the lamotrigine, the large absorption band below 200 nm well-reproduced by the sTDA scheme could also be similarly intense considering more excited states at both TDA and XsTDA levels.

B. Second-harmonic generation of push-pull π-conjugated systems

One recurring problem with the sTD-DFT scheme to evaluate the β_{HRS} is the computation of red-shifted resonance enhancements with respect to the full scheme for push-pull π-conjugated molecules. To circumvent this, we advocated to refit the MNOK two-electron integral parameters to better reproduce reference calculations[15,29,64].

Figure 14 displays β_{HRS} frequency dispersions obtained at BHandHLYP/6-31+G(d) TD-DFT, sTD-DFT, and XsTD-DFT levels of theory for six push-pull π-conjugated molecules. The XsTD-DFT method reproduces almost perfectly TD-DFT β_{HRS} frequency dispersions and in particular the energy position of the resonance enhancement, outperforming the sTD-DFT scheme. This is easily explainable as these resonance enhancements are due to CT states for which the XsTD-DFT scheme is particularly good at reproducing TD-DFT excitation energies. The computational cost to evaluate the first hyperpolarizability at the XsTD-DFT level is extremely low with respect to the full scheme. Computing one single β_{HRS} value for **m-3** with GAMESS[65,66] took 30.9 min[15] on a 8 cores desktop computer (Intel

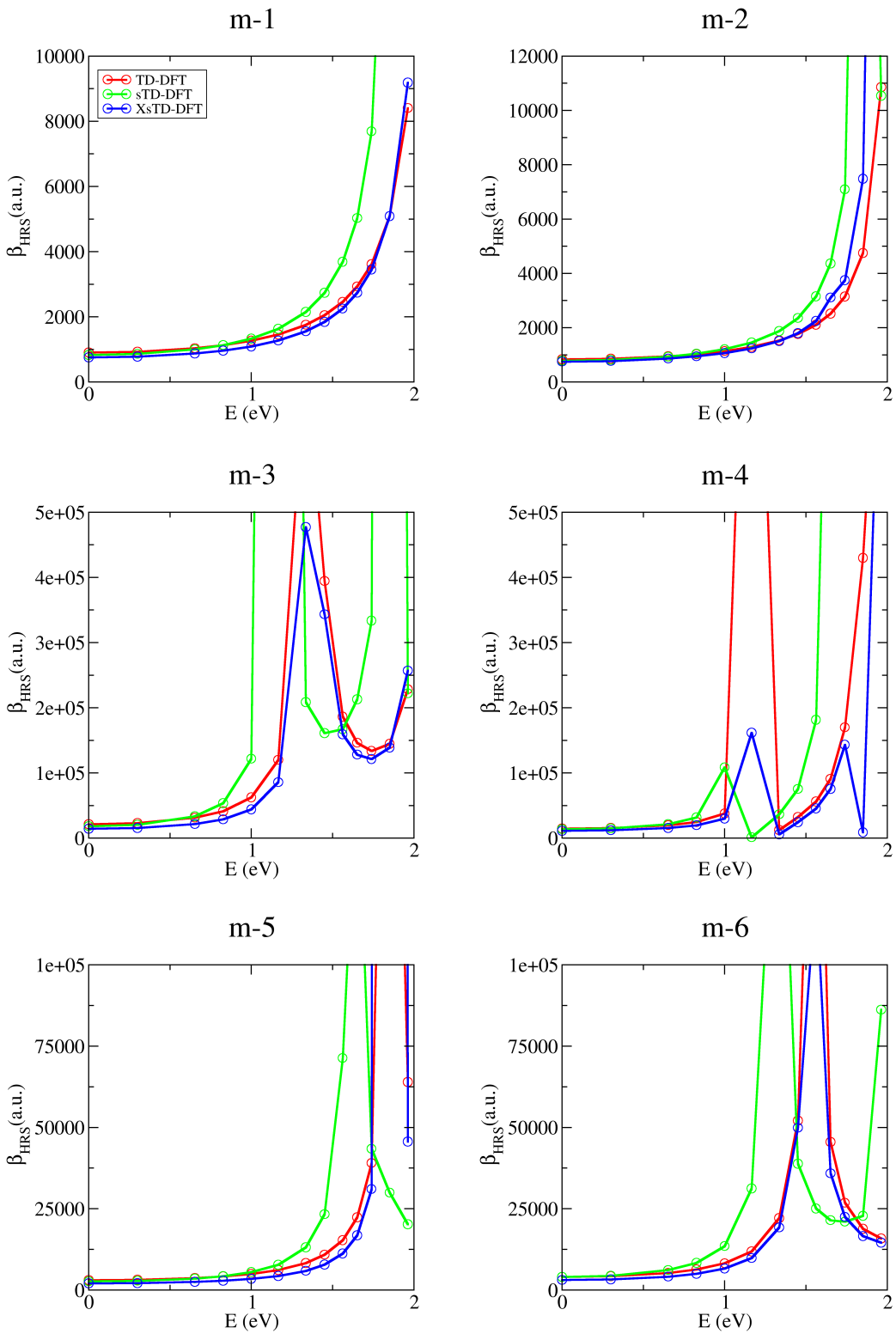

FIG. 14. β_{HRS} frequency dispersions obtained at BHandHLYP/6-31+G(d) TD-DFT, sTD-DFT, and XsTD-DFT levels of theory for the six push-pull π-conjugated molecules. For sTD-DFT and XsTD-DFT calculations, $E_{thresh.} = 15$ eV was used.

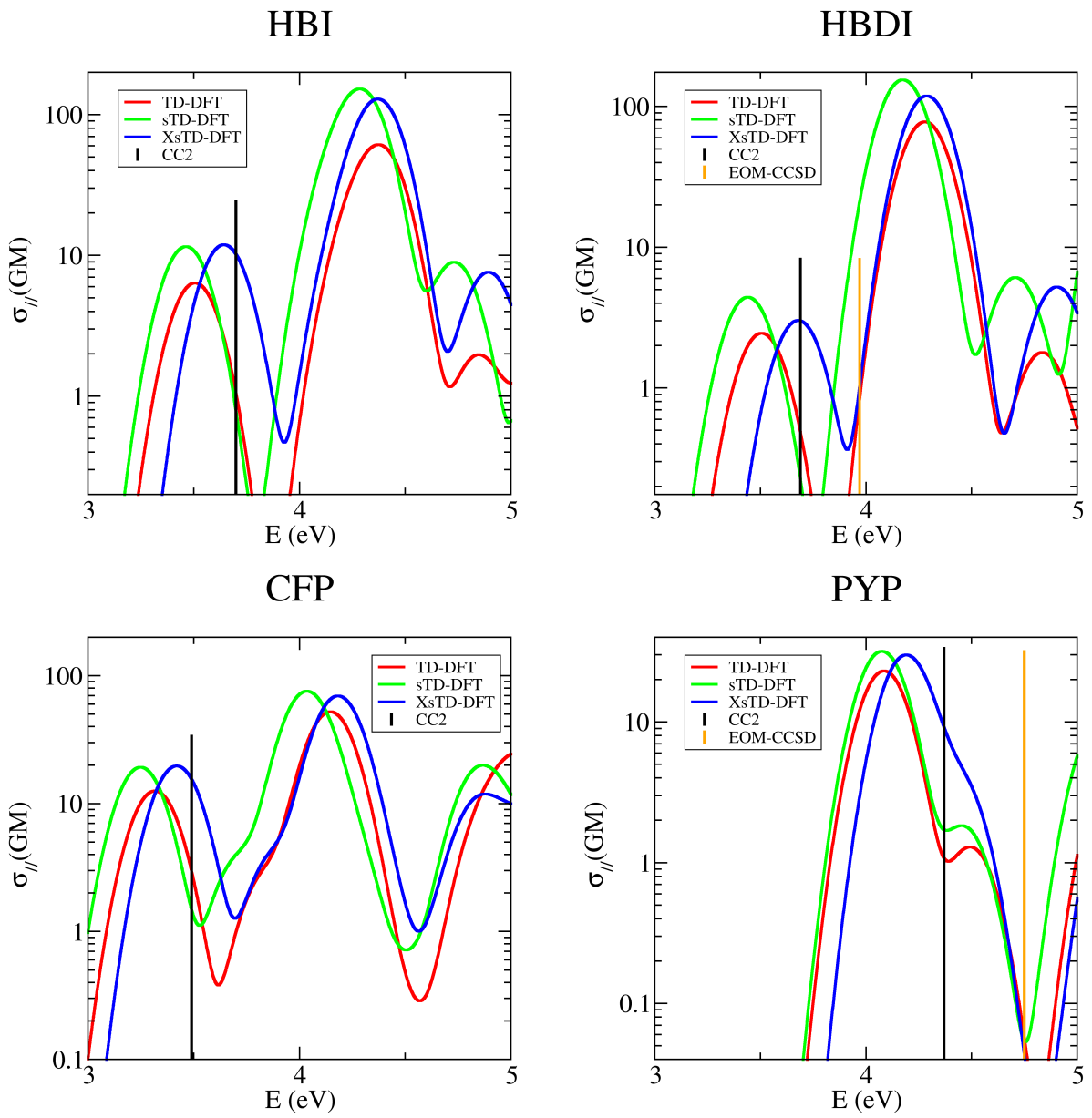

FIG. 15. 2PA spectra for HBI, HBDI, CFP, and PYP computed at B3LYP/6-31+G(d) TD-DFT, sTD-DFT, and XsTD-DFT in comparison to reference RI-CC2/d-aug(-d)-cc-pVDZ or aug-cc-pVDZ excitation energies and 2PA cross-sections for the lowest energy excited state from Beerepoot et al.[39] as well as EOM-CCSD/d-aug(-d)-cc-pVDZ reference calculations from 51, when available.

core i7-6700, 3.40 GHz) while the XsTD-DFT calculation finished in only 5.2 min for 13 β_{HRS} values. The sTD-DFT calculation took 1.9 min.

C. Two-photon absorption

Recently, we showed that calculating absolute 2PA cross-sections (depending on $(2\omega)^2$ and the half width at half maximum for a given line-shape) is inherently difficult for TD-DFT and *de facto* for simplified methods based on TD-DFT.[18] The error for the excitation energy directly impacts the 2PA cross-section. Regarding 2PA strengths (independent of $(2\omega_{ge})^2$), Zaleśny and coworkers[67] demonstrated that global hybrid functionals are not the best choice to compute 2PA strengths. They can reproduce absolute 2PA strengths but have large Pearson correlation coefficients with respect to RI-CC2 results for a set of push-pull π-conjugated systems. Range-separated hybrid functionals underestimate RI-CC2 2PA strengths but better correlate with them. Such functionals will be implemented soon at the XsTD-DFT level. Note that currently, the XsTD-DFT method is extensively benchmarked for 2PA on the benchmark set from Zaleśny and coworkers[67] as well as on compounds from the QUEST database[68–70] at UCLouvain.

Figure 15 compare B3LYP TD-DFT, sTD-DFT, and XsTD-DFT 2PA spectra to RI-CC2 and EOM-CCSD excitation energy and σ^{2PA} for the lowest energy excited state of the four FP chromophores: HBI, HBDI, CFP, and PYP. E_{thresh} = 9 eV was employed for the simplified calculations. A logarithmic scale was used to highlight small 2PA cross-sections. For HBI, the 2PA calculation used 480 basis functions using the 6-31+G(d) basis set. Figure S1 shows that 2PA spectra are almost identical using larger basis sets (aug-cc-pVDZ, 606 basis functions and d-aug-cc-pVDZ, 778 basis functions). Thus, the 6-31+G(d) basis set was selected. TD-DFT 2PA spectral shapes are globally well-reproduced by both simplified methods. sTD-DFT 2PA spectra are slightly red-shifted with respect to TD-DFT ones while XsTD-DFT excitation energies are blue-shifted. Considering the first bright 2P-induced excitation energy for the four systems with respect to RI-CC2 results, MAD of 0.215, 0.263, and 0.086 eV are obtained for TD-DFT, sTD-DFT, and XsTD-DFT, respectively. Comparing orders of magnitudes of 2PA strengths with respect to RI-CC2 ones, MADs for $\log \sigma^{2PA}$ are 0.34 (B3LYP), 0.18 (sB3LYP), and 0.24 (XsB3LYP). This shows that the XsB3LYP excitation energies are in very good agreement with RI-CC2 ones but 2PA strengths are slightly better reproduced by the sB3LYP scheme. Note that for the first bright 2PA excitation of HBDI and PYP, all results are red-shifted with respect to EOM-CCSD excitation energies.

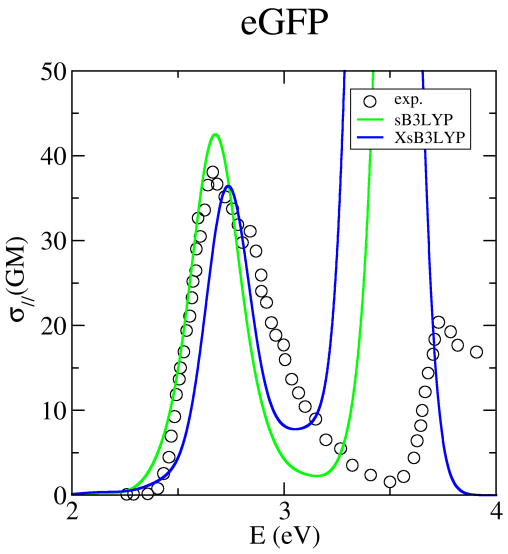

FIG. 16. Experimental 2PA spectrum from Drobizhev et al.[53] in comparison with sB3LYP and XsB3LYP ones computed with the 6-31G(d) basis set, $E_{thresh} = 7$ eV, and N = 2. An energy shift of -0.60 eV was applied the the XsTD-DFT spectrum.

Figure 16 displays the experimental 2PA spectrum recorded by Drobizhev et al.[53] as well as 2PA B3LYP/6-31G(d) sTD-DFT and XsTD-DFT spectra obtained for an eGFP model system (the deprotonated chromophore and its first shell of surrounding residues, 359 atoms). This model stystem was successfully used to reproduce the experimental 2PA spectrum at the sTD-DFT-xTB level of theory.[18] Note that the XsB3LYP 2PA spectrum was globally red-shifted by 0.60 eV. Both sB3LYP and XsB3LYP spectra compare very well with experiment.

V. CONCLUSIONS

This contribution introduced the XsTD-DFT, a computationally efficient method designed to calculate linear and nonlinear optical properties of large systems. This method is based on the sTD-DFT scheme for which semi-empirical integrals are replaced by exact one- and two-center AO two-electron integrals. This new parameter-free method still uses the ZDO approximation with Löwdin-orthogonalized LCAO coefficients to compute MO two-electron integrals. This modification still keeps the XsTD-DFT method computationally efficient with respect to TD-DFT by drastically cutting computational costs by a factor of

20 or more depending on the single energy threshold used. The main difference appears in the construction of **A** and **B** TD-DFT supermatrices where the XsTD-DFT method scales with the number of AOs instead of the number of atoms. Compared to sTD-DFT, these changes were implemented to robustly reproduce TD-DFT results. A TDA variant named XsTDA was also implemented. Both schemes are for the moment limited to global hybrid XC functionals.

To compute excited states, the XsTDA scheme was tested for a set of 77 molecules and compared to TDA using B3LYP, PBE0, BHandHLYP, and M06-2X XC functionals. With respect to the sTDA scheme, the XsTDA method is more robust at reproducing TDA results especially when using XC functionals with large amount of Fock exchange. For example, a MAD of 0.35 eV is obtained when computing excitation energies at the XsM06-2X level of theory while we have a MAD of 0.74 eV with sM06-2X. For oscillator strengths, MADs are also more contained with the XsTDA scheme, especially for large f values. Interestingly, we observed that excitation energy absolute deviations decrease when increasing the size of the system, a behavior most welcomed for a method designed to treat large systems. In 2013, one of us[10] showed that sTDA performs badly when computing $n \rightarrow \pi^*$ and metal-centered $d \rightarrow d$ transitions. The treatment of $n \rightarrow \pi^*$ transitions is not much improved by the XsTDA scheme because of the inherent ZDO approximation that simply neglects one-center exchange integrals. An INDO treatment might solve this problem. Regarding $d \rightarrow d$ transitions, the XsTDA method was able to predict the lowest energy metal-centered $d \rightarrow d$ excitations for ferrocene. Surprisingly, the first one photon-active transition $n \rightarrow Ry(3s)$ of acetone (**3**) was well reproduced by the XsTDA method. Regarding CT states, the XsTDA method robustly reproduces TDA results outperforming the sTDA scheme especially for large amount of Fock exchange. This result really motivates us to implement range-separated hybrid functionals at the XsTD-DFT/XsTDA levels that might confirm the robustness of our new Xs family of methods.

The XsTD-DFT scheme performs equivalently well to compute NLO properties. For a set push-pull π-conjugated systems, we showed that the sTD-DFT method systematically redshifts β_{HRS} resonance enhancements in comparison with the full scheme.[15,64] The XsTD-DFT method fully corrects this behavior thanks to its consistent treatment of CT states with respect to TD-DFT. Both simplified schemes replicate well TD-DFT 2PA spectra for a set of FP chromophores. Note that the XsTD-DFT method provided the best comparison with

respect to RI-CC2 excitation energies for their first bright 2PA excited states. Finally, the experimental 2PA spectrum of eGFP was well reproduced by both sB3LYP and XsB3LYP methods using an eGFP model system.

In view of all these results, we can conclude that the XsTD-DFT/XsTDA methods are robust alternatives to TD-DFT/TDA to compute at a fraction of their computational costs excited state and nonlinear optical response properties. With these new methods, all-atom QC calculations of large systems can now be preformed with a similar accuracy as the full scheme. Such methods can also be very useful for high throughput screening studies considering large ensembles of molecules.

To complement the range of applications of Xs methods, extra implementations are currently ongoing at UCLouvain. The XsTDA/XsTD-DFT gradient is currently being implemented. The support for range-separated hybrid XC functionals by XsTDA/XsTD-DFT methods will be available soon. The extension of XsTD-DFT/XsTDA schemes to compute core to valence excitation is an exciting prospect for which we have already gathered interesting results. An extension of XsTD-DFT/XsTDA schemes to use tight-binding ground states to treat very large systems will be investigated in a near future. A TD-DFT-ris version of the XsTD-DFT scheme should be investigated shortly to reduce the computational cost of the XsTD-DFT scheme.

DATA AVAILABILITY

The data that support the findings of this study are available from the corresponding author upon reasonable request.

ACKNOWLEDGMENTS

M. de W. dedicates this work to his beloved partner Coralie Leroy who passed away from a terrible mitochondrial disease two years ago during the writing of this manuscript. He thanks her for all her love and support during all those years. The authors thank Marilù G. Maraldi for performing the RI-CC2 calculations. This work was supported by the DFG in the framework of the project "Theoretical studies of nonlinear optical properties of fluorescent proteins by novel low-cost quantum chemistry methods" (Nr. 450959503).

REFERENCES

[1]S. Grimme, "Calculation of the electronic spectra of large molecules," in *Reviews in Computational Chemistry* (John Wiley & Sons, Ltd, 2004) Chap. 3, pp. 153–218.

[2]S. Ghosh, P. Verma, C. J. Cramer, L. Gagliardi, and D. G. Truhlar, Chem. Rev. **118**, 7249 (2018).

[3]D. M. Bishop and P. Norman, *Nonlinear Optical Materials in Handbook of Advanced Electronic and Photonic Materials and Devices*, edited by H. S. Nalwa (Academic Press, Burlington, 2001).

[4]M. G. Papadopoulos, A. J. Sadlej, and J. Leszczynski, *Non-linear optical properties of matter* (Springer, 2006).

[5]M. E. Casida, "Time-Dependent Density Functional Response Theory for Molecules," (1995) pp. 155–192.

[6]E. K. U. Gross, J. F. Dobson, and M. Petersilka, "Density functional theory of time-dependent phenomena," in *Density Functional Theory II: Relativistic and Time Dependent Extensions*, edited by R. F. Nalewajski (Springer Berlin Heidelberg, Berlin, Heidelberg, 1996) pp. 81–172.

[7]R. Bauernschmitt and R. Ahlrichs, Chem. Phys. Lett. **256**, 454 (1996).

[8]F. Furche, J. Chem. Phys. **114**, 5982 (2001).

[9]C. Adamo and D. Jacquemin, Chem. Soc. Rev. **42**, 845 (2013).

[10]S. Grimme, J. Chem. Phys. **138**, 244104 (2013).

[11]C. Bannwarth and S. Grimme, Comput. Theor. Chem. **1040-1041**, 45 (2014).

[12]T. Risthaus, A. Hansen, and S. Grimme, Phys. Chem. Chem. Phys. **16**, 14408 (2014).

[13]S. Grimme and C. Bannwarth, J. Chem. Phys. **145**, 054103 (2016).

[14]J. Seibert, J. Pisarek, S. Schmitz, C. Bannwarth, and S. Grimme, Mol. Phys. **117**, 1104 (2019).

[15]M. de Wergifosse and S. Grimme, J. Chem. Phys. **149**, 024108 (2018).

[16]M. de Wergifosse, J. Seibert, and S. Grimme, J. Chem. Phys. **153**, 084116 (2020).

[17]M. de Wergifosse and S. Grimme, J. Chem. Phys. **150**, 094112 (2019).

[18]M. de Wergifosse, P. Beaujean, and S. Grimme, J. Phys. Chem. A **126**, 7534 (2022).

[19]M. de Wergifosse, C. Bannwarth, and S. Grimme, J. Phys. Chem. A **123**, 5815 (2019).

[20]M. de Wergifosse, J. Seibert, B. Champagne, and S. Grimme, J. Phys. Chem. A **123**, 9828 (2019).

[21]M. de Wergifosse and S. Grimme, J. Chem. Theory Comput. **16**, 7709 (2020).

[22]R. Rüger, E. van Lenthe, T. Heine, and L. Visscher, J. Chem Phys. **144**, 184103 (2016).

[23]N. Asadi-Aghbolaghi, R. Rüger, Z. Jamshidi, and L. Visscher, J. Phys. Chem. C **124**, 7946 (2020).

[24]S. Havenridge, R. Rüger, and C. M. Aikens, J. Chem Phys. **158**, 224103 (2023).

[25]G. Giannone and F. Della Sala, J. Chem Phys. **153**, 084110 (2020).

[26]Z. Zhou, F. Della Sala, and S. M. Parker, J. Phys. Chem. Letters **14**, 1968 (2023).

[27]A.-S. Hehn, B. Sertcan, F. Belleflamme, S. K. Chulkov, M. B. Watkins, and J. Hutter, J. Chem. Theory Comput. **18**, 4186 (2022).

[28]Y. Cho, S. J. Bintrim, and T. C. Berkelbach, J. Chem. Theory Comput. **18**, 3438 (2022).

[29]M. de Wergifosse and S. Grimme, J. Phys. Chem. A **125**, 3841 (2021).

[30]K. Nishimoto and N. Mataga, Zeitschrift für Physikalische Chemie **12**, 335 (1957).

[31]K. Ohno, Theor. Chim. Acta **2**, 219 (1964).

[32]G. Klopman, J. Am. Chem. Soc. **86**, 4550 (1964).

[33]R. Pariser and R. G. Parr, J. Chem Phys. **21**, 466 (1953).

[34]L. Goerigk and S. Grimme, J. Chem. Phys. **132**, 184103 (2010).

[35]N. Zadbuke, S. Shahi, A. Jadhav, and S. Borde, Int. J. Pharm. Pharm. Sci. **8**, 234 (2016).

[36]O. S. Keen, I. Ferrer, E. Michael Thurman, and K. G. Linden, Chemosphere **117**, 316 (2014).

[37]S. K. Fadjimata and A. Rabani, IOSR J. Appl. Chem **12**, 51 (2019).

[38]"The stda code can be obtained from: https://github.com/grimme-lab/stda/,".

[39]M. Beerepoot, D. Friese, N. List, J. Kongsted, and K. Ruud, Phys. Chem. Chem. Phys. **17**, 19306 (2015).

[40]M. de Wergifosse and B. Champagne, J. Chem. Phys. **134**, 074113 (2011).

[41]A. Zangwill and P. Soven, Phys. Rev. A **21**, 1561 (1980).

[42]S. Hirata and M. Head-Gordon, Chem. Phys. Lett. **314**, 291 (1999).

[43]F. Wang, C. Y. Yam, and G. Chen, J. Chem. Phys. **126**, 244102 (2007).

[44]A. J. Thorvaldsen, K. Ruud, K. Kristensen, P. Jørgensen, and S. Coriani, J. Chem. Phys. **129**, 214108 (2008).

[45]F. Zahariev and M. S. Gordon, J. Chem. Phys. **140**, 18A523 (2014).

[46]S. M. Parker, D. Rappoport, and F. Furche, J. Chem. Theory Comput. **14**, 807 (2018).

[47]T. Husch, A. C. Vaucher, and M. Reiher, Int. J. Quant. Chem. **118**, e25799 (2018).

[48]Q. Sun, J. Comp. Chem. **36**, 1664 (2015).

[49]H. Langhals, Heterocycles **1**, 477 (1995).

[50]E. Epifanovsky, A. T. B. Gilbert, X. Feng, J. Lee, Y. Mao, N. Mardirossian, P. Pokhilko, A. F. White, M. P. Coons, A. L. Dempwolff, Z. Gan, D. Hait, P. R. Horn, L. D. Jacobson, I. Kaliman, J. Kussmann, A. W. Lange, K. U. Lao, D. S. Levine, J. Liu, S. C. McKenzie, A. F. Morrison, K. D. Nanda, F. Plasser, D. R. Rehn, M. L. Vidal, Z.-Q. You, Y. Zhu, B. Alam, B. J. Albrecht, A. Aldossary, E. Alguire, J. H. Andersen, V. Athavale, D. Barton, K. Begam, A. Behn, N. Bellonzi, Y. A. Bernard, E. J. Berquist, H. G. A. Burton, A. Carreras, K. Carter-Fenk, R. Chakraborty, A. D. Chien, K. D. Closser, V. Cofer-Shabica, S. Dasgupta, M. de Wergifosse, J. Deng, M. Diedenhofen, H. Do, S. Ehlert, P.-T. Fang, S. Fatehi, Q. Feng, T. Friedhoff, J. Gayvert, Q. Ge, G. Gidofalvi, M. Goldey, J. Gomes, C. E. Gonzalez-Espinoza, S. Gulania, A. O. Gunina, M. W. D. Hanson-Heine, P. H. P. Harbach, A. Hauser, M. F. Herbst, M. Hernandez Vera, M. Hodecker, Z. C. Holden, S. Houck, X. Huang, K. Hui, B. C. Huynh, M. Ivanov, A. Jasz, H. Ji, H. Jiang, B. Kaduk, S. Kahler, K. Khistyaev, J. Kim, G. Kis, P. Klunzinger, Z. Koczor-Benda, J. H. Koh, D. Kosenkov, L. Koulias, T. Kowalczyk, C. M. Krauter, K. Kue, A. Kunitsa, T. Kus, I. Ladjanszki, A. Landau, K. V. Lawler, D. Lefrancois, S. Lehtola, R. R. Li, Y.-P. Li, J. Liang, M. Liebenthal, H.-H. Lin, Y.-S. Lin, F. Liu, K.-Y. Liu, M. Loipersberger, A. Luenser, A. Manjanath, P. Manohar, E. Mansoor, S. F. Manzer, S.-P. Mao, A. V. Marenich, T. Markovich, S. Mason, S. A. Maurer, P. F. McLaughlin, M. F. S. J. Menger, J.-M. Mewes, S. A. Mewes, P. Morgante, J. W. Mullinax, K. J. Oosterbaan, G. Paran, A. C. Paul, S. K. Paul, F. Pavosevic, Z. Pei, S. Prager, E. I. Proynov, A. Rak, E. Ramos-Cordoba, B. Rana, A. E. Rask, A. Rettig, R. M. Richard, F. Rob, E. Rossomme, T. Scheele, M. Scheurer, M. Schneider, N. Sergueev, S. M. Sharada, W. Skomorowski, D. W. Small, C. J. Stein, Y.-C. Su, E. J. Sundstrom, Z. Tao, J. Thirman, G. J. Tornai, T. Tsuchimochi, N. M. Tubman, S. P. Veccham, O. Vydrov, J. Wenzel, J. Witte, A. Yamada, K. Yao, S. Yeganeh, S. R. Yost, A. Zech, I. Y. Zhang, X. Zhang, Y. Zhang, D. Zuev, A. Aspuru-Guzik, A. T. Bell, N. A. Besley, K. B. Bravaya, B. R. Brooks, D. Casanova, J.-D. Chai, S. Coriani, C. J. Cramer, G. Cserey, A. E. DePrince, R. A. DiStasio, A. Dreuw, B. D. Dunietz, T. R. Furlani, W. A. Goddard, S. Hammes-Schiffer, T. Head-Gordon, W. J. Hehre, C.-P. Hsu,

T.-C. Jagau, Y. Jung, A. Klamt, J. Kong, D. S. Lambrecht, W. Liang, N. J. Mayhall, C. W. McCurdy, J. B. Neaton, C. Ochsenfeld, J. A. Parkhill, R. Peverati, V. A. Rassolov, Y. Shao, L. V. Slipchenko, T. Stauch, R. P. Steele, J. E. Subotnik, A. J. W. Thom, A. Tkatchenko, D. G. Truhlar, T. Van Voorhis, T. A. Wesolowski, K. B. Whaley, H. L. Woodcock, P. M. Zimmerman, S. Faraji, P. M. W. Gill, M. Head-Gordon, J. M. Herbert, and A. I. Krylov, J. Chem. Phys. **155**, 084801 (2021).

[51]K. D. Nanda and A. I. Krylov, J. Chem. Phys. **142**, 064118 (2015).

[52]M. de Wergifosse, E. Botek, E. De Meulenaere, K. Clays, and B. Champagne, The J. Phys. Chem. B **122**, 4993 (2018).

[53]M. Drobizhev, N. S. Makarov, S. E. Tillo, T. E. Hughes, and A. Rebane, Nat. Meth. **8**, 393 (2011).

[54]K. Aidas, C. Angeli, K. L. Bak, V. Bakken, R. Bast, L. Boman, O. Christiansen, R. Cimiraglia, S. Coriani, P. Dahle, E. K. Dalskov, U. Ekström, T. Enevoldsen, J. J. Eriksen, P. Ettenhuber, B. Fernández, L. Ferrighi, H. Fliegl, L. Frediani, K. Hald, A. Halkier, C. Hättig, H. Heiberg, T. Helgaker, A. C. Hennum, H. Hettema, E. Hjertenæs, S. Høst, I.-M. Høyvik, M. F. Iozzi, B. Jansík, H. J. Aa. Jensen, D. Jonsson, P. Jørgensen, J. Kauczor, S. Kirpekar, T. Kjærgaard, W. Klopper, S. Knecht, R. Kobayashi, H. Koch, J. Kongsted, A. Krapp, K. Kristensen, A. Ligabue, O. B. Lutnæs, J. I. Melo, K. V. Mikkelsen, R. H. Myhre, C. Neiss, C. B. Nielsen, P. Norman, J. Olsen, J. M. H. Olsen, A. Osted, M. J. Packer, F. Pawlowski, T. B. Pedersen, P. F. Provasi, S. Reine, Z. Rinkevicius, T. A. Ruden, K. Ruud, V. V. Rybkin, P. Sałek, C. C. M. Samson, A. S. de Merás, T. Saue, S. P. A. Sauer, B. Schimmelpfennig, K. Sneskov, A. H. Steindal, K. O. Sylvester-Hvid, P. R. Taylor, A. M. Teale, E. I. Tellgren, D. P. Tew, A. J. Thorvaldsen, L. Thøgersen, O. Vahtras, M. A. Watson, D. J. D. Wilson, M. Ziolkowski, and H. Ågren, WIREs Comput. Mol. Sci. **4**, 269 (2014).

[55]"Dalton, a molecular electronic structure program, release dalton2018.0 (2018), see http://daltonprogram.org,".

[56]"TURBOMOLE V7.6 2021, a development of University of Karlsruhe and Forschungszentrum Karlsruhe GmbH, 1989-2007, TURBOMOLE GmbH, since 2007; available from `https://www.turbomole.org`.".

[57]A. Willetts, J. E. Rice, D. M. Burland, and D. P. Shelton, J. Chem. Phys. **97**, 7590 (1992).

[58]J. A. Pople, D. L. Beveridge, and P. A. Dobosh, J. Chem Phys. **47**, 2026 (1967).

[59]J. A. Pople, Trans. Faraday Soc. **49**, 1375 (1953).

[60]D. Jacquemin, V. Wathelet, E. A. Perpète, and C. Adamo, J. Chem. Theory Comput. **5**, 2420 (2009).

[61]D. J. Tozer, J. Chem Phys. **119**, 12697 (2003).

[62]A. J. Cohen, P. Mori-Sánchez, and W. Yang, Chem. Rev. **112**, 289 (2012).

[63]L. Kronik, T. Stein, S. Refaely-Abramson, and R. Baer, J. Chem. Theory Comput. **8**, 1515 (2012).

[64]S. Löffelsender, P. Beaujean, and M. de Wergifosse, WIREs Comp. Mol. Sci. **14**, e1695 (2023).

[65]M. W. Schmidt, K. K. Baldridge, J. A. Boatz, S. T. Elbert, M. S. Gordon, J. H. Jensen, S. Koseki, N. Matsunaga, K. A. Nguyen, S. Su, T. L. Windus, M. Dupuis, and J. A. Montgomery, J. Comput. Chem. **14**, 1347 (1993).

[66]M. S. Gordon and M. W. Schmidt, in *Theory and Applications of Computational Chemistry*, edited by C. E. Dykstra, G. Frenking, K. S. Kim, and G. E. Scuseria (Elsevier, Amsterdam, 2005) pp. 1167 – 1189.

[67]M. Chołuj, M. M. Alam, M. T. P. Beerepoot, S. P. Sitkiewicz, E. Matito, K. Ruud, and R. Zaleśny, J. Chem. Theory Comput. **18**, 1046 (2022).

[68]M. Véril, A. Scemama, M. Caffarel, F. Lipparini, M. Boggio-Pasqua, D. Jacquemin, and P.-F. Loos, WIREs Comp. Mol. Sci. **11**, e1517 (2021).

[69]P.-F. Loos, M. Comin, X. Blase, and D. Jacquemin, J. Chem. Theory Comput. **17**, 3666 (2021).

[70]P.-F. Loos and D. Jacquemin, J. Phys. Chem. A **125**, 10174 (2021).